



Article

Copper–Silver Bimetallic Nanowire Arrays for Electrochemical Reduction of Carbon Dioxide

Yuanxing Wang *, Cailing Niu and Yachuan Zhu

Institute of Advanced Synthesis, School of Chemistry and Molecular Engineering, Jiangsu National Synergetic Innovation Center for Advanced Materials, Nanjing Tech University, Nanjing 211816, Jiangsu, China; hyncljr@163.com (C.N.); zyc_660@163.com (Y.Z.)

* Correspondence: ias_yxwang@njtech.edu.cn

Received: 29 December 2018; Accepted: 27 January 2019; Published: 30 January 2019



Abstract: The electrochemical conversion of carbon dioxide (CO₂) into gaseous or liquid fuels has the potential to store renewable energies and reduce carbon emissions. Here, we report a three-step synthesis using Cu–Ag bimetallic nanowire arrays as catalysts for electrochemical reduction of CO₂. CuO/Cu₂O nanowires were first grown by thermal oxidation of copper mesh in ambient air and then reduced by annealing in the presence of hydrogen to form Cu nanowires. Cu–Ag bimetallic nanowires were then produced via galvanic replacement between Cu nanowires and the Ag⁺ precursor. The Cu–Ag nanowires showed enhanced catalytic performance over Cu nanowires for electrochemical reduction of CO₂, which could be ascribed to the incorporation of Ag into Cu nanowires leading to suppression of hydrogen evolution. Our work provides a method for tuning the selectivity of copper nanocatalysts for CO₂ reduction by controlling their composition.

Keywords: CO₂ reduction; Cu–Ag nanowires; bimetallic nanocatalysts; electrocatalysis

1. Introduction

Carbon dioxide (CO₂) is one of the end products of fossil fuels combustion. The accelerated consumption of fossil fuels leads to accumulated CO₂ concentration in the atmosphere, which is widely considered as one reason for negative environmental consequences [1,2]. Electrochemical reduction can reduce atmospheric CO₂ concentration and convert CO₂ to a variety of useful chemicals, leading to significant changes in the utilization of CO₂ [3–6]. In particular, the electrochemical reduction of CO₂ in fuels and value-added chemicals, a relatively clean method, provides a promising approach to this goal [7,8].

Though the electrochemical reduction of CO₂ on bulk metal electrodes has been studied for decades [9], more recent efforts have focused on nanostructured metallic catalysts for their enhanced catalytic performance over bulk materials [10,11]. Some noble metals, such as Au and Ag, preferably promote the formation of CO [12–15], whereas Pd and Sn preferably form formate [16,17]. Among the commonly studied metals, Cu is a unique catalyst that reduces CO₂ to produce a variety of hydrocarbon and oxygenate products [18,19]. However, there are still challenges in the application of CO₂ reduction to hydrocarbons by copper catalysts, such as low energetic efficiency and poor selectivity of desired products [20,21].

More recently, controlling the composition of nanomaterials has become an efficient way to improve the catalytic activity and selectivity for electrochemical reduction of CO₂ [22]. The bimetallic approach has shown notable results, as it can influence the d-band center of the active components [23]. For instance, Kim et al. found that the selectivity of products could be controlled by tuning the composition of gold–copper bimetallic nanoparticles for electrochemical reduction of CO₂ [24]. Cu nanowires (NWs), a one-dimensional material, have shown higher activity over polycrystalline Cu for

electrochemical reduction of CO₂ owing to their high surface areas [25]. Bimetallic NWs have attracted much attention for their enhanced performance over monometallic NWs for catalytic and electrical applications [26,27]. As Ag is known to be selective for the formation of CO and less expensive than Au [28], it is rational to introduce Ag into Cu NWs to improve their catalytic performance for electrochemical reduction of CO₂.

In this study, we demonstrate the use of galvanic replacement to synthesize Cu–Ag bimetallic NW arrays as catalysts for electrochemical reduction of CO₂. The Cu–Ag NWs were produced by galvanic replacement of Cu NWs with silver, and the starting Cu NWs were obtained by a two-step method involving thermal oxidation of copper mesh and thermal reduction of the grown copper oxide NWs in the presence of hydrogen. The Cu–Ag NWs exhibited a higher selectivity of hydrocarbons and oxygenates over Cu NWs for electrochemical reduction of CO₂. The enhanced catalytic performance was attributed to the incorporation of Ag, which could suppress hydrogen evolution.

2. Experimental Section

2.1. Chemicals and Materials

Copper mesh (99.99%, 100 mesh), and carbon dioxide (CO₂, 99.999%) were used as received. Potassium bicarbonate (KHCO₃, 99.99%) was purchased from Macklin. Ascorbic acid (99.7%) was purchased from Sinopharm Chemical Reagent (Shanghai, China). Silver nitrate (AgNO₃, 99.9999%) was purchased from Sigma Aldrich (St. Louis, United States). Hydrochloric acid was purchased from Shanghai Lingfeng Chemical Reagent (Shanghai, China). Anion exchange membrane was purchased from Tokuyama (Tokyo, Japan). Unless otherwise noted, all chemicals were used as received.

2.2. Copper Nanowire Array Synthesis

CuO/Cu₂O NWs were grown on the copper mesh (100 mesh) adapted by Jiang et al. [29]. A piece of Cu mesh was first washed with 1 mol/L HCl solution for ~30 s to remove the oxide layer. After rinsing with deionized water and drying under N₂ flow, the Cu mesh was placed in a combustion boat and annealed in a muffle furnace at 600 °C for 4 hours. Thermally reduced copper nanowires were obtained by annealing the CuO/Cu₂O NWs at 300 °C for 2 h in a flow of forming gas (5% H₂/N₂, 30 sccm).

2.3. Copper–Silver Nanowire Array Synthesis

The copper NW arrays were immersed in a 20 mL scintillation vial filled with 0.55 mol/L ascorbic acid first. The solution was stirred rapidly for 5 minutes. To produce Cu–Ag nanowire arrays, the copper nanowire arrays were immersed in a solution containing 0.5 mmol/L AgNO₃, and the contents were stirred for 3 minutes. Cu–Ag mesh was produced by a similar method, except copper mesh was used as starting material.

2.4. Material Characterization

Scanning electron microscopy (SEM) images were taken on an FEI Quanta FEG 250 microscope operated at 30 kV. Energy-dispersive X-ray spectroscopy (EDXS) elemental analyses were conducted using an EDXS attachment to the JEOL JEM 2100F transmission electron microscope (TEM). Nickel TEM grids were used for elemental analysis. X-ray diffraction (XRD) patterns were obtained on a Bruker D8 Advance X-ray diffractometer equipped with a Cu K α source ($\lambda = 1.5406 \text{ \AA}$).

2.5. Electrochemical Studies

All electrochemical experiments were carried out in a customized gas-tight three-electrode electrochemical H-cell and a CHI 660E potentiostat. A Pt plate and an Ag/AgCl were used as the counter and reference electrode, respectively. A solution of 0.1 mol/L KHCO₃ was prepared with 18.2 M Ω deionized water and used as the electrolyte. The pH value was measured at 6.8 when the

electrolyte was saturated with CO₂. CO₂ was delivered to the cathode compartment at 10 standard cubic centimeter per minute (sccm). Before each measurement, the electrochemical cell was allowed to purge CO₂ for 30 minutes, for the CO₂ saturation of the electrolyte. The anode and cathode compartment was separated with an anion exchange membrane. All the applied potentials were reported versus reversible hydrogen electrode (RHE) potentials using $E(\text{vs. RHE}) = E(\text{vs. Ag/AgCl}) + 0.199 \text{ V} + 0.059 \text{ V} \times \text{pH}$ with 85% iR drop correction.

The CO₂ electrochemical reaction was performed at ambient temperature and pressure. The gaseous products produced during the reaction were vented into the gas-sampling loop of a gas chromatograph (GC) with CO₂ flow and analyzed online by a GC instrument (GC2060, Shanghai Ruimin) approximately every 15 minutes. The faradaic efficiency (FE) of gaseous products were calculated from the equation:

$$\text{FE} (\%) = (zFvGp_0)/(RT_0i) \times 100\%$$

where z is the theoretical number of e⁻ exchanged to form the gaseous products, v (vol%) is gaseous products volume concentration in the exhaust gas from the electrochemical cell, G (mL/min) is the gas flow rate, i is the cell current, $F = 96,485 \text{ C/mol}$, $p_0 = 1.01 \times 10^5 \text{ Pa}$, $R = 8.314 \text{ J/(mol K)}$, and $T_0 = 273.15 \text{ K}$ [30].

The liquid products formed during the reaction were analyzed offline by a nuclear magnetic resonance spectrometer (Bruker Avance 400M, Karlsruhe, Germany). For analysis, the electrolyte was mixed with D₂O to form 90%:10% volume ratio solution and a known concentration of dimethyl sulfoxide as an internal standard. The ¹H spectrum was measured with a water suppression method. FE of liquid products was calculated according to the equation:

$$\text{FE} (\%) = znF/Q \times 100 \%$$

where z is the theoretic number of e⁻ exchanged to form the liquid products, n is the moles of products, Q is the total charges applied, and $F = 96,485 \text{ C/mol}$ [31].

3. Results and Discussion

Figure 1 depicts the three-step synthesis process of Cu–Ag bimetallic NW arrays on the copper mesh. To prepare Cu NW arrays, a two-step method including thermal oxidation and reduction was adapted [25,29]. First, CuO/Cu₂O NW arrays were synthesized by annealing copper mesh in ambient air. Then, the subsequent thermal reduction of CuO/Cu₂O NW arrays was performed in a flow of forming gas to form Cu NW arrays. Last, the Cu NW arrays were immersed into an AgNO₃ solution to yield Cu–Ag NW arrays for CO₂ reduction. Detailed information about the synthesis can be found in the Experimental Section.

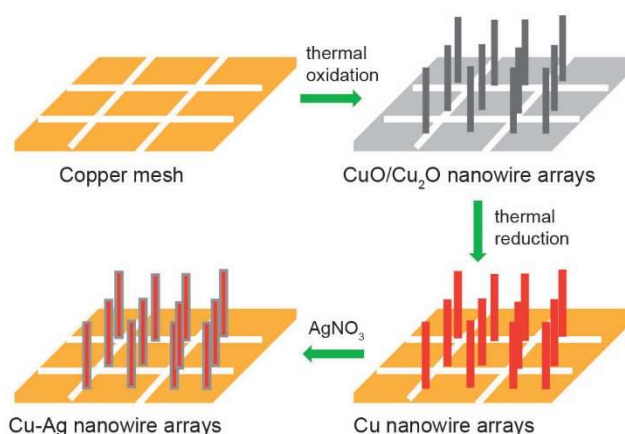


Figure 1. Schematic illustration of the synthesis of Cu–Ag nanowire (NW) arrays.

Figure 2a,b shows the scanning electron microscope (SEM) images of synthesized CuO/Cu₂O NW arrays. The CuO/Cu₂O NWs were mainly grown vertically to the surface of the Cu mesh. Typical diameters of the produced CuO/Cu₂O NWs were in the range of 50–100 nm with lengths up to 30 μm. The SEM images of the thermally reduced Cu NWs are shown in Figure 2c,d. Based on these images, the thermally reduced Cu NWs generally maintained the dimensions of the CuO/Cu₂O NWs, despite some deformation of the head of the NWs. Additional SEM images can be found in the Supporting Information.

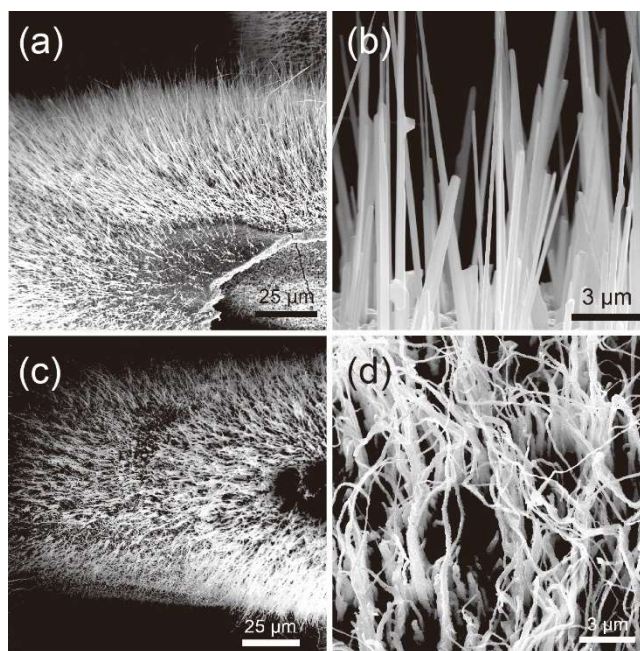


Figure 2. Low- and high-magnification SEM images of (a,b) as-synthesized CuO/Cu₂O NWs and (c,d) thermally reduced Cu NWs.

To verify the crystal structure of the Cu mesh, annealed CuO/Cu₂O NWs, and reduced Cu NWs, powder X-ray diffraction (XRD) measurements were made on representative samples. Figure 3 illustrates the XRD patterns of Cu mesh after annealing and reveals characteristic CuO reflections at 32.6, 35.6, 38.8, 48.9, 53.6, 58.3, 61.6, 66.3, 68.2, 72.5, and 75.4° (Joint Committee on Powder Diffraction Standards (JCPDS) card No. 05-0661), Cu₂O reflections at 29.7, 36.5, 42.4, 73.6, and 77.4° (JCPDS card No. 65-3288), and metallic Cu reflections at 43.4, 50.6, and 74.3° (JCPDS card No. 65-9473). XRD pattern collected from reduced Cu NWs shows peaks of cubic Cu same as pristine Cu mesh. The XRD data indicate that annealing copper mesh in air produced high density CuO/Cu₂O NWs, while the subsequent thermal reduction actually made cubic Cu NWs on the copper mesh. Additional details about these SEM and XRD measurements can be found in the Experimental Section.

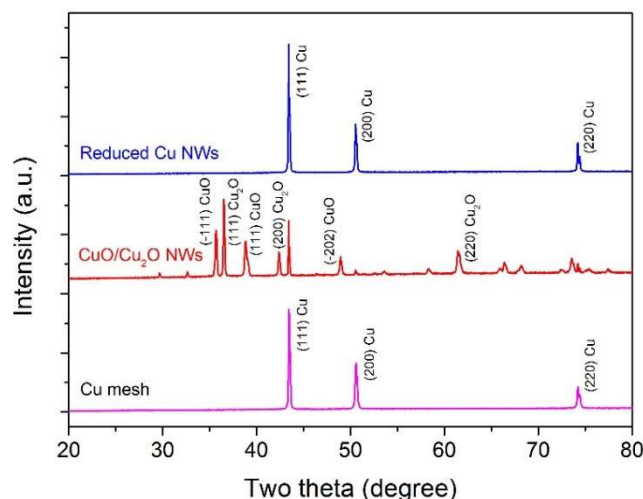


Figure 3. X-ray diffraction patterns of pristine copper mesh (magenta), annealed CuO NWs (red), and thermally reduced Cu NWs (blue).

In recent years, galvanic replacement reactions have been applied as a synthetic tool for bimetallic nanomaterials [32,33]. By dipping Cu NWs into an AgNO_3 solution, Cu–Ag NW arrays were obtained via galvanic replacement of silver according to the following equation [34,35]: $\text{Cu}_{(s)} + 2\text{Ag}^+ \rightarrow \text{Cu}^{2+} + 2\text{Ag}_{(s)}$. Figure 4a,b shows the representative high-magnification SEM images of starting Cu NWs and obtained Cu–Ag NW arrays, respectively. The morphologies of these Cu–Ag NWs were similar to the Cu NWs (i.e., diameter of ~100 nm with length of up to 30 μm), despite some deposition on the surface of the Cu NWs. The rough surface could be ascribed to the large lattice mismatch between Cu and Ag [36]. To verify the crystal structure of Cu–Ag NWs, power XRD measurement was performed. The above metallic Cu diffraction peaks all appeared in the pattern of Cu–Ag NWs, but a new peak at 38.2° was consistent with (111) plane of cubic Ag (JCPDS No. 04-0783), suggesting some amount of Ag in the Cu–Ag NWs (Figure 4c). At this point, energy-dispersive X-ray spectroscopy (EDXS) measurement was carried out to determine the elemental information of the resulted bimetallic NWs. Based on Figure 4c, the Ag–Cu ratio was ~1:10 in the Cu–Ag bimetallic NWs. The EDXS mapping figure (Figure S3) indicated the uniform distribution of Cu and Ag on the NWs. The SEM, XRD, and EDXS data together indicated the successful synthesis of Cu–Ag bimetallic NWs. Detailed information about the synthesis can be found in the experimental section. Additional SEM images can be found in the supporting information.

Having established the synthesis of Cu–Ag NWs, electrochemical reduction of CO_2 was conducted in CO_2 -saturated 0.1 mol/L KHCO_3 electrolyte at ambient temperature and pressure. CO_2 reduction experiments were performed in an electrolysis cell with the cathode and anode compartment separated by an anion exchange membrane, preventing the oxidation of CO_2 reduction products. The cathodic compartment was purged with CO_2 at a constant flow rate and vented into a gas chromatograph (GC) for quantification of gaseous products. The liquid products were analyzed by ^1H nuclear magnetic resonance (NMR) spectroscopy after the completion of experiments.

The activity and selectivity of Cu NWs, Cu–Ag NWs, Cu mesh and Cu–Ag mesh for CO_2 electroreduction were studied. Figure 5a shows the linear sweep voltammograms (LSV) of Cu NWs in comparison to the LSV of Cu–Ag NWs, using geometric current density as a comparison standard. Based on the LSV measurements, the Cu–Ag NWs generally exhibited a higher catalytic activity (larger negative current density and lower negative onset potential) over Cu NWs. To compare the long-term performance of each NW, their total geometric current density vs. time at various potentials are shown in Figure 5b–d, respectively. During the reaction, the decline in current densities for Cu NWs at various potentials indicates their unstableness for CO_2 reduction. This phenomenon was more obvious at more negative potentials, such as -0.8 V vs. reversible hydrogen electrode (RHE; all potentials reported here

are with respect to this reference). However, Cu–Ag NWs catalysts exhibited a steady-state current at constant potentials, which indicates the alloyed NWs were stable in the current electrochemical reaction conditions. The bimetallic NWs achieved a current density of ~ 6 mA/cm² at relatively low overpotential (-0.6 V), which was even higher than the reported current density by using Ag NWs and Cu₂O-derived films as catalysts [28,37]. The Cu–Ag NWs showed higher catalytic activity for CO₂ electroreduction over Cu NWs which could be ascribed to the addition of the Ag ingredient into Cu NWs, implying the impact of composition effects of Cu NWs catalysts for CO₂ reduction. Additional details about the electrochemical studies can be found in the Experimental Section and Supporting Information.

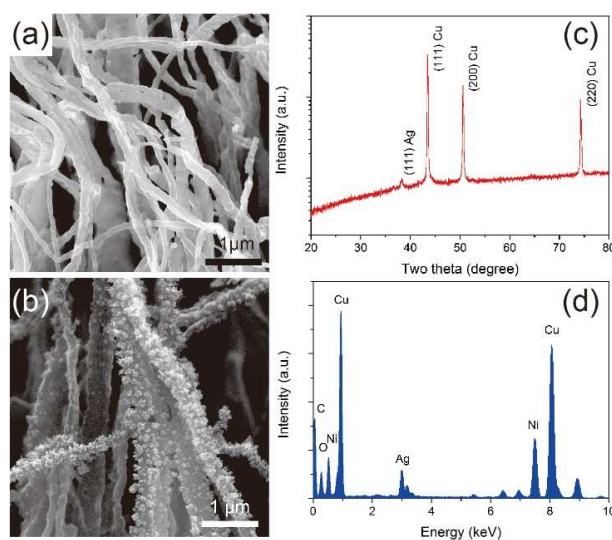


Figure 4. High-magnification SEM images of (a) thermally reduced Cu NWs, and (b) as-synthesized Cu–Ag NWs; (c) XRD pattern of the Cu–Ag NWs; (d) EDXS spectrum of the Cu–Ag NWs (Ni peak was from nickel TEM grid).

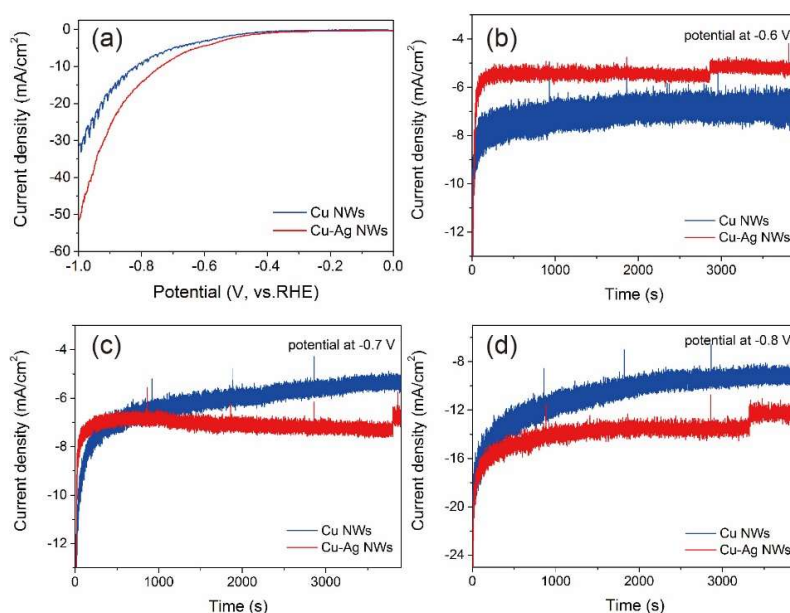


Figure 5. (a) Linear sweep voltammetry of electrochemical CO₂ reduction on the Cu NWs and the Cu–Ag NWs with 5 mV/s scan rate. CO₂ reduction activity on the Cu NWs and the Cu–Ag NWs at different potentials: (b) -0.6 V, (c) -0.7 V, and (d) -0.8 V.

Figure 6 summarizes the faradaic efficiency (FE) of the desired products for the Cu NWs and Cu–Ag NWs at constant potentials during CO₂ electroreduction. Figures S4–S6 summarize the selectivity of major products in the tests of long-term performance. For gaseous products, Ag–Cu NWs showed lower selectivity of H₂ than the Cu NWs, along with higher selectivity of CO, C₂H₄, and C₂H₂ at all studied potentials. For liquid products, Ag–Cu NWs presented a higher selectivity of total liquid products over the Cu NWs. For example, the Cu NWs exhibited a H₂ FE of 65%, a CO FE of 8%, and a formate FE of 17%, while the Cu–Ag NWs showed a H₂ FE of 46%, a CO FE of 14%, and a formate FE of 24% at -0.7 V. In general, the Cu–Ag NWs exhibited enhanced catalytic selectivity of products towards CO₂ electroreduction than that of the Cu NWs. The Cu–Ag NWs exhibited the best catalytic performance among all the studied materials (Figures S7–S12). It is important to note that the Cu NWs showed similar H₂ selectivity as that of the Cu–Ag NWs at -0.8 V; this most likely reflects the mass transport limitations at high current density (e.g., >10 mA/cm²) rather than the intrinsic selectivity of these catalysts [18]. The enhancement in catalytic performance of the Cu–Ag NWs over Cu NWs may originate from different electronic structure by alloying a silver element into the copper composition [24]. Based on the density function theory (DFT) calculated binding energy of CO on the metal surface, Ag favors desorption of CO (an important reactive intermediate in the CO₂ electroreduction) on its surface [38]. In addition, Ag adsorbs hydrogen weakly and the sluggish reaction–intermediate formation slows down the hydrogen evolution reaction [39]. The lower selectivity of H₂, as well as higher selectivity of CO, hydrocarbons, and oxygenates after introducing Ag into Cu NWs, could be ascribed to the reasons mentioned above.

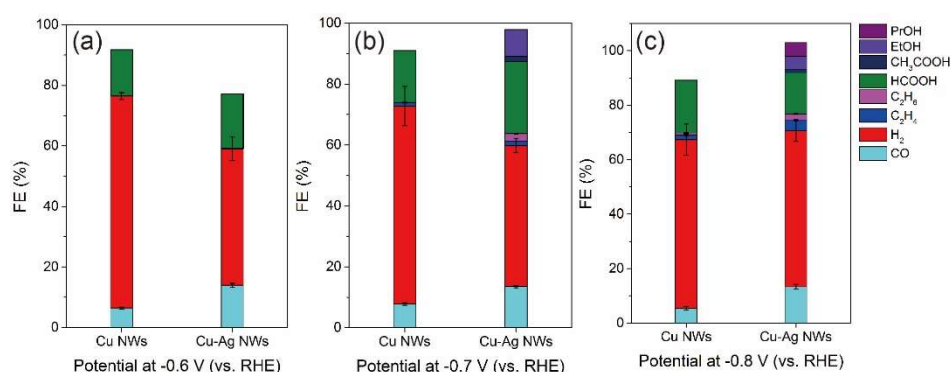


Figure 6. Faradaic efficiency (FE) of the major products for the Cu NWs and the Cu–Ag NWs at different applied potentials: -0.6 V (a), -0.7 V (b) and -0.8 V (c).

4. Conclusions

In summary, a simple three-step method was used to produce Cu–Ag NW arrays as electrocatalysts for CO₂ reduction. CuO/Cu₂O NWs were first grown by thermal oxidation of copper mesh, then thermal reduction was performed to form Cu NWs. By galvanic replacement with silver, Cu–Ag NWs were obtained while maintaining similar morphology and structure of the parent Cu NWs. The Cu–Ag NWs exhibited enhanced catalytic selectivity of hydrocarbons and oxygenates towards CO₂ electroreduction over Cu NWs, attributed to the incorporation of Ag. Our work highlights the potential opportunity to tune the activity and selectivity of copper catalysts for CO₂ electroreduction by controlling their composition.

Supplementary Materials: The following are available online at <http://www.mdpi.com/2079-4991/9/2/173/s1>, Figure S1: High-magnification SEM images of as-synthesized CuO/Cu₂O NWs. Figure S2: Low-magnification SEM images of as-synthesized Cu–Ag NWs. Figure S3: EDXS mapping figure of the Cu–Ag NWs (a) Cu distribution, (b) Ag distribution, and (c) TEM image. Figure S4: Time-dependent FE of major gaseous products for the Cu NWs and the Cu–Ag NWs at -0.6 V (vs. RHE). Figure S5: Time-dependent FE of major gaseous products for the Cu NWs and the Cu–Ag NWs at -0.7 V (vs. RHE). Figure S6: Time-dependent FE of major gaseous products for the Cu NWs and the Cu–Ag NWs at -0.8 V (vs. RHE). Figure S7: X-ray diffraction patterns of pristine copper mesh (blue) and Cu–Ag mesh (red). Figure S8: Linear sweep voltammetry of electrochemical

CO₂ reduction of the Cu mesh and the Cu–Ag mesh. Figure S9: CO₂ reduction activity on the Cu mesh and the Cu–Ag mesh at different potentials. Figure S10: FE of the major products for the Cu mesh and the Cu–Ag mesh at –0.6 V (vs. RHE). Figure S11: FE of the major products for the Cu mesh and the Cu–Ag mesh at –0.7 V (vs. RHE). Figure S12: FE of the major products for the Cu mesh and the Cu–Ag mesh at –0.8 V (vs. RHE).

Author Contributions: C.N. and Y.Z. synthesized and characterized the nanomaterials, and analyzed the data. Y.W. designed the experiments and wrote the paper.

Funding: This research was funded by Nanjing Tech University, grant number 39837130. The APC was funded by Nanjing Tech University.

Acknowledgments: The authors are grateful for financial support by a Startup Grant (39837130) from Nanjing Tech University and a SICAM Fellowship by Jiangsu National Synergetic Innovation Center for Advanced Materials. The authors thank Dr. Dunwei Wang for his helpful guidance and input. Y.W. thanks office of China Postdoc Council and Nanjing Tech University for an international postdoctoral exchange fellowship.

Conflicts of Interest: The authors declare no conflict of interest.

References

1. Wang, W.-H.; Himeda, Y.; Muckerman, J.T.; Manbeck, G.F.; Fujita, E. CO₂ Hydrogenation to Formate and Methanol as an Alternative to Photo- and Electrochemical CO₂ Reduction. *Chem. Rev.* **2015**, *115*, 12936–12973. [[CrossRef](#)] [[PubMed](#)]
2. Khezri, B.; Fisher, A.C.; Pumera, M. CO₂ Reduction: The Quest for Electrocatalytic Materials. *J. Mater. Chem. A* **2017**, *5*, 8230–8246. [[CrossRef](#)]
3. Benson, E.E.; Kubiak, C.P.; Sathrum, A.J.; Smieja, J.M. Electrocatalytic and Homogeneous Approaches to Conversion of CO₂ to Liquid Fuels. *Chem. Soc. Rev.* **2009**, *38*, 89–99. [[CrossRef](#)] [[PubMed](#)]
4. Rakowski Dubois, M.; Dubois, D.L. Development of Molecular Electrocatalysts for CO₂ Reduction and H₂ Production/Oxidation. *Acc. Chem. Res.* **2009**, *42*, 1974–1982. [[CrossRef](#)] [[PubMed](#)]
5. Schneider, J.; Jia, H.; Muckerman, J.T.; Fujita, E. Thermodynamics and Kinetics of CO₂, CO, and H⁺ Binding to the Metal Centre of CO₂ Reduction Catalysts. *Chem. Soc. Rev.* **2012**, *41*, 2036–2051. [[CrossRef](#)] [[PubMed](#)]
6. Jones, J.-P.; Prakash, G.K.S.; Olah, G.A. Electrochemical CO₂ Reduction: Recent Advances and Current Trends. *Isr. J. Chem.* **2014**, *54*, 1451–1466. [[CrossRef](#)]
7. Lu, Q.; Jiao, F. Electrochemical CO₂ Reduction: Electrocatalyst, Reaction Mechanism, and Process Engineering. *Nano Energy* **2016**, *29*, 439–456. [[CrossRef](#)]
8. Wang, Y.; Niu, C.; Wang, D. Metallic Nanocatalysts for Electrochemical CO₂ Reduction in Aqueous Solutions. *J. Colloid Interface Sci.* **2018**, *527*, 95–106. [[CrossRef](#)]
9. Hori, Y. Electrochemical CO₂ Reduction on Metal Electrodes. In *Modern Aspects of Electrochemistry*; Springer: New York, NY, USA, 2008; pp. 89–189.
10. Lu, Q.; Rosen, J.; Jiao, F. Nanostructured Metallic Electrocatalysts for Carbon Dioxide Reduction. *ChemCatChem* **2015**, *7*, 38–47. [[CrossRef](#)]
11. Wang, Y.; Liu, J.; Wang, Y.; Al-Enizi, A.M.; Zheng, G. Tuning of CO₂ Reduction Selectivity on Metal Electrocatalysts. *Small* **2017**, *13*, 1701809. [[CrossRef](#)]
12. Chen, Y.; Li, C.W.; Kanan, M.W. Aqueous CO₂ Reduction at Very Low Overpotential on Oxide-Derived Au Nanoparticles. *J. Am. Chem. Soc.* **2012**, *134*, 19969–19972. [[CrossRef](#)] [[PubMed](#)]
13. Zhu, W.; Zhang, Y.-J.; Zhang, H.; Lv, H.; Li, Q.; Michalsky, R.; Peterson, A.A.; Sun, S. Active and Selective Conversion of CO₂ to CO on Ultrathin Au Nanowires. *J. Am. Chem. Soc.* **2014**, *136*, 16132–16135. [[CrossRef](#)] [[PubMed](#)]
14. Kim, C.; Jeon, H.S.; Eom, T.; Jee, M.S.; Kim, H.; Friend, C.M.; Min, B.K.; Hwang, Y.J. Achieving Selective and Efficient Electrocatalytic Activity for CO₂ Reduction Using Immobilized Silver Nanoparticles. *J. Am. Chem. Soc.* **2015**, *137*, 13844–13850. [[CrossRef](#)] [[PubMed](#)]
15. Ma, M.; Trzeźniewski, B.J.; Xie, J.; Smith, W.A. Selective and Efficient Reduction of Carbon Dioxide to Carbon Monoxide on Oxide-Derived Nanostructured Silver Electrocatalysts. *Angew. Chem. Int. Ed.* **2016**, *55*, 9748–9752. [[CrossRef](#)] [[PubMed](#)]
16. Zhang, S.; Kang, P.; Meyer, T.J. Nanostructured Tin Catalysts for Selective Electrochemical Reduction of Carbon Dioxide to Formate. *J. Am. Chem. Soc.* **2014**, *136*, 1734–1737. [[CrossRef](#)] [[PubMed](#)]

17. Min, X.; Kanan, M.W. Pd-Catalyzed Electrohydrogenation of Carbon Dioxide to Formate: High Mass Activity at Low Overpotential and Identification of the Deactivation Pathway. *J. Am. Chem. Soc.* **2015**, *137*, 4701–4708. [[CrossRef](#)] [[PubMed](#)]
18. Li, C.W.; Kanan, M.W. CO₂ Reduction at Low Overpotential on Cu Electrodes Resulting from the Reduction of Thick Cu₂O Films. *J. Am. Chem. Soc.* **2012**, *134*, 7231–7234. [[CrossRef](#)]
19. Reske, R.; Mistry, H.; Behafarid, F.; Roldan Cuenya, B.; Strasser, P. Particle Size Effects in the Catalytic Electroreduction of CO₂ on Cu Nanoparticles. *J. Am. Chem. Soc.* **2014**, *136*, 6978–6986. [[CrossRef](#)]
20. Peterson, A.A.; Abild-Pedersen, F.; Studt, F.; Rossmeisl, J.; Norskov, J.K. How Copper Catalyzes the Electroreduction of Carbon Dioxide into Hydrocarbon Fuels. *Energy Environ. Sci.* **2010**, *3*, 1311–1315. [[CrossRef](#)]
21. Kortlever, R.; Shen, J.; Schouten, K.J.P.; Calle-Vallejo, F.; Koper, M.T.M. Catalysts and Reaction Pathways for the Electrochemical Reduction of Carbon Dioxide. *J. Phys. Chem. Lett.* **2015**, *6*, 4073–4082. [[CrossRef](#)]
22. Zhang, L.; Zhao, Z.-J.; Gong, J. Nanostructured Materials for Heterogeneous Electrocatalytic CO₂ Reduction and their Related Reaction Mechanisms. *Angew. Chem. Int. Ed.* **2017**, *56*, 11326–11353. [[CrossRef](#)] [[PubMed](#)]
23. Chen, D.; Yao, Q.; Cui, P.; Liu, H.; Xie, J.; Yang, J. Tailoring the Selectivity of Bimetallic Copper–Palladium Nanoalloys for Electrocatalytic Reduction of CO₂ to CO. *ACS Appl. Energy Mater.* **2018**, *1*, 883–890. [[CrossRef](#)]
24. Kim, D.; Resasco, J.; Yu, Y.; Asiri, A.M.; Yang, P. Synergistic Geometric and Electronic Effects for Electrochemical Reduction of Carbon Dioxide using Gold–Copper Bimetallic Nanoparticles. *Nat. Commun.* **2014**, *5*, 4948. [[CrossRef](#)] [[PubMed](#)]
25. Raciti, D.; Livi, K.J.; Wang, C. Highly Dense Cu Nanowires for Low-Overpotential CO₂ Reduction. *Nano Lett.* **2015**, *15*, 6829–6835. [[CrossRef](#)] [[PubMed](#)]
26. Alia, S.M.; Pivovar, B.S.; Yan, Y. Platinum-Coated Copper Nanowires with High Activity for Hydrogen Oxidation Reaction in Base. *J. Am. Chem. Soc.* **2013**, *135*, 13473–13478. [[CrossRef](#)] [[PubMed](#)]
27. Niu, Z.; Cui, F.; Yu, Y.; Becknell, N.; Sun, Y.; Khanarian, G.; Kim, D.; Dou, L.; Dehestani, A.; Schierle-Arndt, K.; et al. Ultrathin Epitaxial Cu@Au Core–Shell Nanowires for Stable Transparent Conductors. *J. Am. Chem. Soc.* **2017**, *139*, 7348–7354. [[CrossRef](#)]
28. Liu, S.; Wang, X.-Z.; Tao, H.; Li, T.; Liu, Q.; Xu, Z.; Fu, X.-Z.; Luo, J.-L. Ultrathin 5-Fold Twinned Sub-25nm Silver Nanowires Enable Highly Selective Electroreduction of CO₂ to CO. *Nano Energy* **2018**, *45*, 456–462. [[CrossRef](#)]
29. Jiang, X.; Herricks, T.; Xia, Y. CuO Nanowires Can Be Synthesized by Heating Copper Substrates in Air. *Nano Lett.* **2002**, *2*, 1333–1338. [[CrossRef](#)]
30. Zhu, W.; Michalsky, R.; Metin, Ö.; Lv, H.; Guo, S.; Wright, C.J.; Sun, X.; Peterson, A.A.; Sun, S. Monodisperse Au Nanoparticles for Selective Electrocatalytic Reduction of CO₂ to CO. *J. Am. Chem. Soc.* **2013**, *135*, 16833–16836. [[CrossRef](#)]
31. Ma, M.; Djanashvili, K.; Smith, W.A. Controllable Hydrocarbon Formation from the Electrochemical Reduction of CO₂ over Cu Nanowire Arrays. *Angew. Chem. Int. Ed.* **2016**, *55*, 6680–6684. [[CrossRef](#)]
32. Lu, X.; McKiernan, M.; Peng, Z.; Lee, E.P.; Yang, H.; Xia, Y. Noble-Metal Nanotubes Prepared via a Galvanic Replacement Reaction Between Cu Nanowires and Aqueous HAuCl₄, H₂PtCl₆, or Na₂PdCl₄. *Sci. Adv. Mater.* **2010**, *2*, 413–420. [[CrossRef](#)]
33. Mohl, M.; Dobo, D.; Kukovec, A.; Konya, Z.; Kordas, K.; Wei, J.; Vajtai, R.; Ajayan, P.M. Formation of CuPd and CuPt Bimetallic Nanotubes by Galvanic Replacement Reaction. *J. Phys. Chem. C* **2011**, *115*, 9403–9409. [[CrossRef](#)]
34. Stewart, I.E.; Ye, S.; Chen, Z.; Flowers, P.F.; Wiley, B.J. Synthesis of Cu–Ag, Cu–Au, and Cu–Pt Core–Shell Nanowires and Their Use in Transparent Conducting Films. *Chem. Mater.* **2015**, *27*, 7788–7794. [[CrossRef](#)]
35. Xia, X.; Wang, Y.; Ruditskiy, A.; Xia, Y. 25th Anniversary Article: Galvanic Replacement: A Simple and Versatile Route to Hollow Nanostructures with Tunable and Well-Controlled Properties. *Adv. Mater.* **2013**, *25*, 6313–6333. [[CrossRef](#)] [[PubMed](#)]
36. Weng, W.-L.; Hsu, C.-Y.; Lee, J.-S.; Fan, H.-H.; Liao, C.-N. Twin-Mediated Epitaxial Growth of Highly Lattice-Mismatched Cu/Ag Core-Shell Nanowires. *Nanoscale* **2018**, *10*, 9862–9866. [[CrossRef](#)] [[PubMed](#)]
37. Janáky, C.; Hursán, D.; Endrődi, B.; Chanmanee, W.; Roy, D.; Liu, D.; de Tacconi, N.R.; Dennis, B.H.; Rajeshwar, K. Electro- and Photoreduction of Carbon Dioxide: The Twain Shall Meet at Copper Oxide/Copper Interfaces. *ACS Energy Lett.* **2016**, *1*, 332–338. [[CrossRef](#)]

38. Kuhl, K.P.; Hatsukade, T.; Cave, E.R.; Abram, D.N.; Kibsgaard, J.; Jaramillo, T.F. Electrocatalytic Conversion of Carbon Dioxide to Methane and Methanol on Transition Metal Surfaces. *J. Am. Chem. Soc.* **2014**, *136*, 14107–14113. [[CrossRef](#)]
39. Yao, Z.; Yan, J.; Mietek, J.; Zhang, Q.S. Advancing the Electrochemistry of the Hydrogen-Evolution Reaction through Combining Experiment and Theory. *Angew. Chem. Int. Ed.* **2015**, *54*, 52–65.



© 2019 by the authors. Licensee MDPI, Basel, Switzerland. This article is an open access article distributed under the terms and conditions of the Creative Commons Attribution (CC BY) license (<http://creativecommons.org/licenses/by/4.0/>).